

A CHROMATIN STRUCTURE BASED MODEL ACCURATELY PREDICTS DNA REPLICATION TIMING IN HUMAN CELLS

Yevgeniy Gindin^{1,2}, Manuel S. Valenzuela³, Mirit I. Aladjem⁴, Paul S. Meltzer^{1*} and Sven Bilke¹

¹Genetics Branch, Center for Cancer Research, Bethesda, MD 20892, USA

²Graduate Program in Bioinformatics, Boston University, Boston, MA 02215, USA

³Department of Biochemistry and Cancer Biology, School of Medicine, Meharry Medical College, Nashville, TN 37208, USA

⁴Laboratory of Molecular Pharmacology, National Cancer Institute, Bethesda, MD 20892, USA

*To whom correspondence should be addressed at:

National Cancer Institute

37 Convent Dr.

Bethesda, MD 20982-4265

pmeltzer@mail.nih.gov

301-496-5266 (Ph)

301-402-3241 (Fax)

Abstract

The metazoan genome is replicated in precise cell lineage specific temporal order. However, the mechanism controlling this orchestrated process is poorly understood as no molecular mechanisms have been identified that actively regulate the firing sequence of genome replication. Here we develop a mechanistic model of genome replication capable of predicting, with accuracy rivaling experimental repeats, observed empirical replication timing program in humans. In our model, replication is initiated in an uncoordinated (time-stochastic) manner at well-defined sites. The model contains, in addition to the choice of the genomic landmark that localizes initiation, only a single adjustable parameter of direct biological relevance: the number of replication forks. We find that DNase hypersensitive sites are optimal and independent determinants of DNA replication initiation. We demonstrate that the DNA replication timing program in human cells is a robust emergent phenomenon that, by its very nature, does not require a regulatory mechanism determining a proper replication initiation firing sequence.

Introduction

In eukaryotes, DNA replication is a tightly regulated process that follows a strict temporal program (Taylor, 1960; Masai *et al*, 2010). This timing program is intimately associated with key aspects of cell biology, including cell differentiation (Hiratani *et al*, 2004; Hansen *et al*, 2010; Hiratani *et al*, 2010), cancer progression (Donley & Thayer, 2013a; Fritz *et al*, 2012; Ryba *et al*, 2012), the 3D conformation of cellular DNA (Ryba *et al*, 2012; Moindrot *et al*, 2012; Ryba *et al*, 2010) and the formation of cytogenetic aberrations (De & Michor, 2011). Whereas the genome-wide replication program in eukaryotes appears nearly deterministic, individual replication initiation events display a large degree of stochasticity (Bechhoefer & Rhind, 2012). An important step in resolving this apparent discrepancy was to recognize a formal analogy between DNA replication and nucleation in one dimension (Kolmogorov, 1937; Jun *et al*, 2005), which serves as the foundation for most of today's mathematical models of DNA replication. But while the molecular components of DNA replication modeled in this formalism are mostly conserved across the domains of life, it was found that the mechanism of recognition and regulation of initiation sites varies greatly, even between lower and higher eukaryotes (Aladjem, 2007).

Particularly amenable to modeling are extreme examples of initiation site recognition: random and well-characterized. *Xenopus Laevis* is a representative of random initiation site selection. Modeling efforts for this organism, which need not take into account locations of initiation sites, have helped to provide theoretical answers to the so-called random completion problem (Blow *et al*, 2001; Herrick *et al*, 2002; Yang & Bechhoefer, 2008), and the global increase of the replication initiation rate throughout the S-phase suggested as one possible solution has later been confirmed experimentally and described as a universal feature across eukaryotic replication (Goldar *et al*, 2009). *Saccharomyces cerevisiae*

occupies the other end of the initiation site recognition spectrum. Its quite well-characterized and efficient replication initiation sites have helped to extract a number of parameters relevant for modeling efforts, such as the average and the variance of the firing time distribution for individual initiation sites. Based on such estimates, mathematical models were able to reproduce the global timing program found in yeast (Lygeros *et al*, 2008; Yang *et al*, 2010; de Moura *et al*, 2010) thus demonstrating how the deterministic timing program emerges from individually stochastic initiation events.

Initiation site selection in metazoan genomes lies somewhere between these two extreme cases. While here too, replication initiation occurs at discrete sites in the genome, the metazoan replicator remains relatively poorly characterized, as even the most efficient sites fire in only a fraction of cell cycles (Valenzuela *et al*, 2011; Martin *et al*, 2011). This makes it more difficult to directly observe location and amplitudes of initiation (Besnard *et al*, 2012; Martin *et al*, 2011) or to extract this information from replication timing data (Baker *et al*, 2012b), contributing to the dearth of timing models for metazoan cells. Beyond these technical difficulties of obtaining a comprehensive set of robust parameters, a model built around tuning a large number of parameters (at least one for each of the 100,000 estimated initiation sites (Pope *et al*, 2013) in human cells) would remain somewhat unsatisfactory. It would also sidestep the question of what factors determine replication timing and could therefore not explain timing plasticity. Moreover, parameters for such a model would have to be re-determined for every cell-state. To address these challenges, we built a minimal model and identified a genomic marker that can be utilized to predict, rather than reproduce, genome-scale DNA replication timing profiles at high resolution with an accuracy (Pearson's $r=0.92$) rivaling that of experimental repeats ($r=0.94$) performed in different laboratories. We use our model to demonstrate that the replication timing program can be explained by the approximate location of initiation sites alone, regardless of other factors such as exact initiation probabilities and that initiation sites are optimally localized by DNase hypersensitive (HS)

sites.

Results

Mechanistic model of DNA replication

The focus of this study was to understand and predict the dynamic DNA replication timing program of human cells. Here we took a reductionist modeling approach, including only essential components while omitting all features not required to model the timing program. In the resulting model (**Figures 1A, S1**), a number N of rate-limiting factors independently select genomic locations and initiate replication (if the location has not yet been replicated) with probabilities specified for that location by an initiation probability landscape (IPLS). Thus, the probability of replication initiation at a given genomic location x is the product of the probability of a rate-limiting factor selecting one of the unreplicated competent initiation sites at time t , the initiation probability assigned to that location by the IPLS and the number of available (unengaged) rate-limiting factors at time t .

Since the result of each simulation is determined by the choice of the input IPLS, the biological question of what determines the DNA replication timing program can be addressed by identifying the IPLS that most accurately predicts experimentally observed data. Here, human replication timing data published in (Hansen *et al*, 2010) and (Ryba *et al*, 2012) were used for this benchmark. Both datasets report the average behavior of cell populations. We compared our model's prediction, averaged over millions of Monte Carlo simulated cell cycles, to these benchmark datasets. The concordance between predictions generated by the optimal model (see below) and the experimental data is striking at the 500bp resolution used in our simulations (**Figures 1B and S2**), recapitulating peaks and valleys of replication timing on a chromosome-wide scale (**Figure 1C**).

Predictive power of static genomic features

Earlier studies (Valenzuela *et al*, 2011; Martin *et al*, 2011; Cayrou *et al*, 2011) had indicated that DNA replication initiation is more likely to occur in the vicinity transcription start sites (TSSs). Thus, as a starting point, we tested the predictive capacity of an IPLS where we assigned a constant, time-independent high initiation probability to all TSSs annotated in RefSeq (Pruitt *et al*, 2005) and low probabilities everywhere else (see Supplement for further discussion). Despite the simplicity of these assumptions, the resulting timing prediction is quite similar (average $r=0.69$ across four cell lines **Figure 2A**) to the experimental data. Testing other sequence features that were previously associated with replication initiation generates similarly good predictions: CpG islands (Meyer *et al*, 2013) ($r=0.64$), GC content (Meyer *et al*, 2013) ($r=0.58$), and predicted G4-quadruplexes (Besnard *et al*, 2012) ($r=0.55$) (**Figures 2A and S3**). Remarkably, an IPLS based on a structural feature of the DNA molecule, namely its solvent-accessible surface (Greenbaum *et al*, 2007), produced profiles ($r=0.51$) only slightly less predictive than some of the other, more commonly discussed factors (**Figures 2A and S3**). However, such invariant properties of the genome cannot account for timing plasticity observed across cell types (Hansen *et al*, 2010). We therefore hypothesized that dynamic genomic landmarks would generate models better suited to capture differentiation lineage-specific timing plasticity.

DNase hypersensitive sites are the main determinants of DNA replication timing

Utilizing the recently published (Rosenbloom *et al*, 2013; ENCODE Project Consortium and others, 2011) ENCODE data, we generated IPLSs from all 167 cell-specific datasets available for the cell lines in the Hansen data by assigning an initiation probability proportional to the ENCODE amplitude, simulated the timing patterns and compared the results to the empirical DNA replication timing data for corresponding cells (Table S1). Nearly one-half (77 out of 167) of the probed ENCODE marks produce

better predictive models compared to the best (TSS based) static model (**Table 1** and **Figure S4**). Notably, the gene expression based model (AffyExonArray, $r=0.75$) did not show a measurably improved accuracy in comparison to the static TSS model ($r=0.69$). The top-ranking model ($r=0.87$) is based on an IPLS derived from DNase HS sites. This is followed by models derived from activating chromatin marks such as H3k9ac ($r=0.83$), H3k4me2 ($r=0.83$) or transcription factor binding (e.g. JunD $r=0.86$).

We hypothesized that the ability of more than one epigenetic mark to predict DNA replication timing with high fidelity is a consequence of the fact that many chromatin marks tend to co-localize (Thurman *et al*, 2012) and that, in isolation, some marks would lose much of their predictive value. To test this possibility, we performed simulations based on reduced sets, where mutually co-localized marks were removed (**Figures 2B** and **S5**). Remarkably, among the tested top-ranking genomic marks selected for this analysis (histone H3K4me2, H3K9ac, transcription factor JunD and DNase HS sites) *only* DNase HS sites fully retained their ability to predict replication timing in *all* pairwise comparisons. For *all* other marks, accuracy of the timing prediction was substantially reduced when removing overlaps with DNase HS sites, even when accounting for the reduced set size. We further explored whether these same marks co-localize with empirically determined DNA replication initiation sites (Besnard *et al*, 2012). Our results show that JunD, H3K4me2, and H3K9ac sites overlap DNA replication origins only so long as they also overlap DNase HS sites (**Figure S6**). We therefore conclude, based on the available data, that DNase HS is the main independent determinant of replication timing. This conclusion is further supported by observing that almost half of the DNase HS sites in HeLa (47%, $P < 1E-6$, OR=5.0) and IMR90 (47%, $P < 1E-6$, OR=3.8) cells are located within 500 bases of empirically determined initiation sites (Besnard *et al*, 2012). Also, the non-trivial distribution of initiation sites across chromosomes, with the density of initiation sites varying substantially between chromosomes, is

closely recapitulated by DNase HS sites (Figure 2C and S7).

DNA replication timing plasticity across cell lineages and species and its alteration as a result of chromosomal fusions

Replication timing shows remarkable plasticity across differential lineages (Donley & Thayer, 2013b) and in cancer cells (Ryba *et al*, 2012). Utilizing DNase HS data for three cell lines (BJ, GM06990, K562), for which matching experimental timing and DNase HS data were available, we performed DNA replication simulations and hierarchical clustering of the simulated and experimental data (**Figure 3A**). The model predictions tightly cluster with the experimental data for the matching cell and also recapitulate the closer relatedness of GM06990 and K562 cells (both of hematopoietic origin) in comparison to BJ (fibroblast). Using stringent parameters (see Methods), we identified 60 genes (Table S2) in regions with replication timing variable regions between GM06990 and K562 cells and found a significant enrichment for interferon and haemoglobin complexes (DAVID (Huang *et al*, 2009) P-value 3.3E-12 and 2.3E-10, respectively), including the human β -globin locus (**Figure 3B**) – in line with phenotypic properties of these cells.

The accuracy of our model predictions in human cells suggested that the same mechanism will likely work in other mammalian cells. Currently, the lack of simultaneous availability of both, replication timing and DNase HS data for the same cells, limits the ability for a broader analysis. To test the applicability of our model to mouse embryonic fibroblast cells, we compared replication timing predictions generated from DNase HS sites in NIH/3T3 cells (ENCODE Project Consortium and others, 2011) to observed timing data in MEF cells (Hiratani *et al*, 2010). The average Pearson correlation between model prediction and experimental replication data is 0.85 (**Figure S8**), confirming that our model can be extended to other metazoan cells.

Recurrent chromosomal fusions are found in many cancers (Rowley, 1973; Delattre *et al*, 1992; Tomlins *et al*, 2005). In acute lymphoblastic leukemia, the well-characterized t(12;21)(p13;q22); *ETV6-RUNX1* fusion is accompanied by an abrupt change in DNA replication timing near the fusion site (Ryba *et al*, 2012). Our model reproduces this behavior when inducing (see Supplement) an *in silico* t(12;21)(p13;q22) translocation in GM06990 lymphoblastoid cells (**Figure 3C**). This behavior is also reproduced when comparing replication timing at the *in-silico* induced breakpoint in GM06990 cells with observed replication timing in REH cells, which harbor the translocation (**Figure S9**). The results show that replication timing is not determined at the site of the breakpoint. Instead, the timing pattern arises from the combined influence of the DNase HS sites situated on either side of the break. The discontinuity, observed experimentally and reproduced in the simulation, is the result of mapping physical coordinates of the rearranged chromosome 12 onto the normal genome.

Modeling parameters

The proposed model has remarkably few parameters. In addition to an IPLS and an optional technical variable (see below) there is only one adjustable parameter, namely the maximum number (N) of replication forks that can be active simultaneously. As N is not set *a priori* (**Figure S10**) we performed a series of simulations identifying, for each chromosome, the optimal N that generates the closest match to the experimental data. We find that the optimal N grows linearly with chromosome length at a rate of 1 fork per 1.3 mega bases (**Figure 3D**), compatible with the assumption that the stochastic process governing replication does not substantially differ between chromosomes. Subsequently, we used the estimate from the linear regression curve in this experiment for N . With this setting, the predicted median length of the S-phase is 5965 (mean=6134) simulation steps (**Figure 3E**) in GM06990 cells. In real human cells, replication forks move at a speed of about 50 bases per second (Alberts *et al*, 2008). With a 500bp model-resolution (and two forks moving in opposite directions in

each simulation step) the predicted median wall-clock time for the S-phase is $t = 5965 \text{ steps} * 500 \text{ bases} / (50 \text{ bases} / \text{second}) / (2 \text{ step}) = 8.3 \text{ hours}$, in line with the experimentally observed duration of 6-10 hours. The optional technical variable mentioned previously governs the simulation of a flow-sorter, which in laboratory experiments divides asynchronously replicating cells into S-phase fractions (Ryba *et al*, 2011). As the actual gate settings used were not available (Hansen *et al*, 2010), numerical optimizations (see Supplement) were used, further improving the similarity of the best (DNase HS based) simulated models from $r=0.89$ (with 5 equidistant gates in GM06990 cells) to $r=0.92$, a level approaching the limit of experimental noise ($r=0.94$ between experiments performed in different laboratories).

DNA replication timing is highly robust

With only a single adjustable biological parameter, and thus no real risk of over-fitting the data, the accuracy of our model predictions is exceptionally high, suggesting a high degree of robustness of the proposed model. One potential limitation is the completeness of genomic annotations. To test its importance, we built a series of models by randomly sub-sampling DNase HS annotations. The predictions were essentially unchanged despite removing up to 75% of DNase HS sites with the accuracy degrading gradually beyond this point (**Figure S11A**). We conclude that the local replication timing program emerges from the collective contribution of adjacent initiation sites, and, as a systems phenomenon, it is largely independent from individual sites.

The model also shows a large degree of insensitivity with respect to specific modeling choices. We wondered how strongly the specifics of assigning probabilities in the IPLS based on ENCODE amplitudes affects the simulation results. For the simulations presented so far, the local initiation probability was set to be proportional to the ENCODE amplitude. We tried alternate assignment functions (**Figure S11B**) which resulted in only insignificant changes in the accuracy of the model

prediction (linear $r=0.86$, square $r=0.86$, square-root $r=0.84$) and even when assigning the same *constant* value to all sites ($r=0.86$). On the molecular level in real cells, this implies that, once a site is competent to initiate, the probability that it is going to do so does not substantially affect the global replication timing program. We conclude that the relevant information provided by the ENCODE data, with regard to DNA replication timing, is *location* while *amplitude* is irrelevant. In our early simulations, we had included a small background initiation rate outside of the high efficiency initiation sites demarcated by DNase HS sites. This choice, too, was found to not affect the accuracy of the model prediction (see Supplement), even when assigning a zero background initiation rate, i.e. when initiation exclusively occurred at high efficiency sites (**Figure S12**).

Discussion

Here we present a mechanistic model that fully predicts replication timing in human cells, without the need to adjust any parameters for new cell types. Once the number of rate limiting factors and the genomic landmark that optimally generates the initiation probability landscape had been identified, the same constant choices produced accurate timing predictions for any tested cell type. Designed in a reductionist spirit, we attempted to omit all details from the model that are not required to understand the timing program (**Figures S1A & B**). We wondered, if the replication fork collision mechanism in the model, which dynamically determines the distance a fork travels, could be removed by instead using the density of DNase HS sites in the vicinity (see Supplement) to assign a replication time. All such models produced substantially worse predictions (**Figure S13** and Supplemental material) indicating that the collision mechanism is a required aspect of the model. Therefore, while genomic regions dense in DNase HS sites delineate early DNA replication regions (**Figure 1C**), they are not sufficient, on their own, to predict DNA replication timing.

An explicit separation of replication into licensing and initiation steps proved also to be unnecessary. This separation is known to be an essential molecular mechanism to avoid over-replication: licensing occurs exclusively in late M / early G1 by assembly of the so-called pre-replication complex (PreRC) at potential initiation sites, with initiation occurring later in the S-phase by conversion of the PreRC into bi-directional replication forks through phosphorylation and recruitment of other factors (Machida *et al*, 2005). In our model, the IPLS subsumes these two steps (over-replication itself is prevented by explicitly keeping track of replicated regions), the initiation probability at a given site represents the product of the biological probabilities to first assemble and later activate the PreRC. The above described intrinsic robustness of the model with respect to the assignment of probabilities in the IPLS is remarkable in this context. It implies that the factor dominating the timing program is the selection of the *location* of PreRC assemblies. Our model predicts (**Figure S11B**) that the empirical timing pattern will emerge even if all PreRCs, once assembled, have the *same*, constant probability of being subsequently activated unless the site is passively replicated. While, to our knowledge, this possibility has not been tested in metazoan cells, it has broadly been shown to be the case in yeast (Yang *et al*, 2010), where a majority of initiation sites were demonstrated to have a “potential initiation efficiency”, with the initiation probability remaining larger than 0.9 after correcting for passive replication.

Remarkably, we were not required to introduce a time-dependent IPLS in order to precisely predict the global replication timing pattern. Earlier models (Yang *et al*, 2010; Hyrien & Goldar, 2010) used location and explicit time-dependent initiation rates $I(x,t)$ to force individual initiation sites to fire, on average, at the right time to reproduce the global timing pattern. While these approaches elegantly reconcile the orchestrated global replication timing program with the stochastic nature of individual initiation events, they do not ultimately address what determines the local initiation timing. Instead, they *reproduce*, but not *predict*, replication timing. This is because these models rely on existing timing

data, for each cell type, in order to fit a large number of variables, one or more for each initiation site. In contrast, in the model presented here, the global timing program results from the spatial distribution of initiation sites, a determination of individual firing rates was therefore not necessary. Once the genomic landmark that optimally locates initiation sites, DNase HS, was determined, timing could be predicted for all cell types. We expect that the basic mechanism described here will also work in other metazoan cells. Indeed, we found an excellent agreement between our model prediction and experimental timing data in mouse embryonic fibroblast cells (**Figure S8**).

Another important reason to use a time dependent, globally increasing initiation rate throughout S-phase in earlier models is to stabilize the S-phase length, thus avoiding the random completion problem (Blow *et al*, 2001; Herrick *et al*, 2002; Yang & Bechhoefer, 2008). These predictions were confirmed by a recent analysis (Goldar *et al*, 2009), uncovering a universal behavior of the global initiation firing rate across a number of species. How does this reconcile with the time-independent IPLS presented here? The firing rate in our model depends not only on the explicitly time-independent IPLS, but also on the number of unengaged rate-limiting factors, which dynamically changes over time, as well as on the search time to find unreplicated origins, which differs between early and late replicating regions as a result of the difference in the density of initiation sites. A numerical analysis of the global initiation rate (**Figure S15**), shows a remarkable qualitative similarity to the universal patterns described in (Goldar *et al*, 2009). It will be interesting to see if it is necessary to extend our model by including a more detailed replication factor diffusion process, such as the sub-diffusive model discussed in (Gauthier & Bechhoefer, 2009), in order to obtain a quantitative match with experimentally determined global initiation rates in human cells.

We identified DNase hypersensitivity as the optimal IPLS predicting the DNA replication timing in

metazoan cells. This suggests that DNA replication timing is largely determined mechanistically: locally by DNA accessibility as the dominant factor modulating the likelihood of forming competent initiation complexes and globally by the process of colliding replication forks – a reduced representation of the known molecular processes. This interpretation implies a causal relationship, where the distribution of accessible genome regions determines DNA replication timing. Recently, a tight correlation, although significantly weaker (Pearson's $r=0.8$) compared to the best models tested here, between replication timing and the first eigenvector of the HiC contact probability matrix has been reported (Ryba *et al*, 2010), suggesting that the 3D genome organization may play a prominent role in DNA replication timing for example via replication factories or by determining the boundaries of replication domains (Baker *et al*, 2012a). It may, therefore, seem surprising that our accurately predictive model does not require any reference to the spatial genomic organization. It could be that both phenomena, the distribution of DNase HS and 3D conformation, have a common cause. Yet, it is generally believed that DNase HS sites are established by transcription factors dislocating and/or limiting the movement of histones (Felsenfeld *et al*, 1996). It therefore seems reasonable to speculate that the distribution of DNase HS sites might itself contribute to the control of the genomic conformation.

In summary, provided with a proper “initiation probability landscape” – a mathematical construct that encodes the location information, the model predicts the replication timing program and recapitulates cell-specific timing patterns, including abnormal timing behavior in cancer cells. These results strongly support the concept that replication timing is a stochastic process ultimately determined by chromatin structure, which itself is a consequence of the topological organization of genes and functional regulatory elements on the chromosome as encoded in the DNA sequence.

Materials and Methods

Software implementation

The custom-written software (Replicon) is capable to simulating genome replication and recording various associated measurements, such as DNA replication timing. Replicon is written in C++ and can be executed in a multi-threaded mode. In our experiments, a typical simulation of a human genome-wide DNA replication profile took about 15 minutes when executed in parallel: 22 simulations each running on a 4-core, 2.93 GHz Linux node.

Simulated replication time assignment to genome coordinates

The simulation consists of millions of simulated asynchronous cells. The assignment of replication time to genome coordinates starts by first separating the cell population, according to each cell's DNA content, into one of six bins (akin to a flow-sorter sort). The replication time is calculated for each genome coordinate (500bp resolution) by taking the average of the product of the bin number (1 through 6) and the number of times the genome coordinate in question was observed in each bin.

Flow sorter gating optimization

We used a simulated annealing algorithm to approximate DNA flow-sorter bin boundaries with the objective to minimize the Euclidean distance between simulated and experimentally derived DNA replication timing profile. Starting from a state where flow-sorter bin boundaries were randomized, replication timing was simulated based on DNase DGF data for GM06990 cells. The neighboring state was calculated by perturbing a randomly chosen bin boundary. The new boundary value was chosen from Normal distribution, where μ was set to the old boundary and σ to a value of 1.

IPLS Generation

Utilizing a 500bp resolution, the probability of initiating replication at any given genomic location was set to either a scaled value of an attribute of interest or to a background frequency of $1E-4$, whichever was greater. Scaling was achieved using the formula $x / \max(x)$, where x is the attribute of interest. All DNA replication initiation landscapes, unless stated otherwise, were generated from a local copy of the UCSC ENCODE database (Rosenbloom *et al*, 2013), where the data attribute 'score' was used as the attribute of interest. For GC-content IPLS, the probability of DNA replication initiation was scaled to

the 'sumData' attribute of the 'gc5Base' annotation table. For CpG island IPLS, the probability of DNA replication initiation was scaled to the 'obsExp' attribute of the 'cpgIslandExt' annotation table. For DNA G-quadruplex (G4) IPLS, the probability of DNA replication initiation was scaled to the length of the G4 motif. The G4 motifs were identified using a regular expression as described in (Todd *et al*, 2005). ORChID IPLS was based on 'wgEncodeBuOrchidV1.bigWig' annotation file available at the UCSC Genome Browser (<http://genome.ucsc.edu/>), where the intensities of hydroxyl radical accessibility were averaged over non-overlapping 500bp windows. The transcription start site (TSS) IPLS, was set to a constant probability of 1.0 for every genomic region annotated as 'txStart' in the 'refGene' table.

Generation of Reduced-Model IPLSs

For each set of genome annotations in a pair-wise comparison, we identified and removed co-localized genome regions, generating the 'Subtract Overlap' reduced model for each model in the comparison. The 'Subtract Random' model was generated by removing randomly chosen genome regions from each model in the comparison, such that the number of regions in 'Subtract Overlap' and 'Subtract Random' models were equal.

In silico ETV6-RUNX1 Translocation

We generated t(12;21)(p13;q22) chromosomal translocation *in silico* by joining GM06990 DNase DGF data for chromosomes 12 and 21 – producing an *ETV6*-*RUNX* fusion gene using molecularly mapped breakpoint coordinates (Wiemels *et al*, 2000). We then simulated replication timing for two fused chromosome products and compared simulated replication timing data for translocated and un-translocated chromosome 12.

Robustness

The effect of deleting DNase HS sites was investigated using DNase DGF data available for GM06990 cells. At each iteration of the algorithm, we erased an ever-increasing fraction of DNase sites and generated a corresponding DNA replication initiation landscape.

DNA Replication Plasticity Regions

DNA replication plasticity regions were identified using custom-developed software. First, a DNA replication difference profile was derived for a given pair of DNA replication timing profiles by

subtracting one DNA replication profile from another for matching genome coordinates. The distribution of differences was observed to follow Normal distribution. Using the Normal distribution, a P-value was assigned to every 500bp non-overlapping genome bin (the resolution of our model) in the difference profile. A DNA replication plasticity region was identified as such if at least 3 consecutive bins were assigned a P-value of 0.001 or less.

Acknowledgements

This research was supported by the Intramural Research Program of the NIH, National Cancer Institute, Center for Cancer Research. We thank Sean Davis, Kevin Gardner, and Subhajyoti De for discussions.

Author Contributions

Y.G., and S.B. wrote the manuscript and designed experiments with significant contributions made by M.S.V., M.I.A., and P.S.M.; Y.G. and S.B. designed and performed statistical analyses and interpreted the data, Y.G. developed optimization routines; S.B. conceived the proposed model and implemented the simulator, S.B. and P.S.M. conceived the study and supervised the work.

Conflict of Interest

All authors declare no competing financial interest. Correspondence and requests for materials should be addressed to pmeltzer@mail.nih.gov.

REFERENCES

- Aladjem MI (2007) Replication in context: dynamic regulation of DNA replication patterns in metazoans. *Nat. Rev. Genet.* **8**: 588–600
- Alberts B, Wilson JH & Hunt T (2008) Molecular Biology of the Cell 5th ed. Garland Science
- Baker A, Audit B, Chen C-L, Moindrot B, Leleu A, Guilbaud G, Rappailles A, Vaillant C, Goldar A, Mongelard F, D'Aubenton-Carafa Y, Hyrien O, Thermes C & Arneodo A (2012a) Replication fork polarity gradients revealed by megabase-sized U-shaped replication timing domains in human cell lines. *PLoS Comput. Biol.* **8**: e1002443
- Baker A, Audit B, Yang SC-H, Bechhoefer J & Arneodo A (2012b) Inferring Where and When Replication Initiates from Genome-Wide Replication Timing Data. *Phys. Rev. Lett.* **108**: 268101
- Bechhoefer J & Rhind N (2012) Replication timing and its emergence from stochastic processes. *Trends Genet.* **28**: 374–81
- Besnard E, Babled A, Lapasset L, Milhavet O, Parrinello H, Dantec C, Marin J-M & Lemaitre J-M (2012) Unraveling cell type-specific and reprogrammable human replication origin signatures associated with G-quadruplex consensus motifs. *Nat. Struct. Mol. Biol.* **19**: 837–44
- Blow JJ, Gillespie PJ, Francis D & Jackson D a (2001) Replication origins in Xenopus egg extract Are 5-15 kilobases apart and are activated in clusters that fire at different times. *J. Cell Biol.* **152**: 15–25
- Cayrou C, Coulombe P, Vigneron A, Stanojcic S, Ganier O, Peiffer I, Rivals E, Puy A, Laurent-Chabalier S, Desprat R & Méchali M (2011) Genome-scale analysis of metazoan replication origins reveals their organization in specific but flexible sites defined by conserved features. *Genome Res.* **21**: 1438–49
- De S & Michor F (2011) DNA replication timing and long-range DNA interactions predict mutational landscapes of cancer genomes. *Nat. Biotechnol.* **29**: 1103–8
- Delattre O, Zucman J, Plougastel B, Desmaze C, Melot T, Peter M, Kovar H, Joubert I, de Jong P & Rouleau G (1992) Gene fusion with an ETS DNA-binding domain caused by chromosome translocation in human tumours. *Nature* **359**: 162–165
- Donley N & Thayer MJ (2013a) DNA replication timing, genome stability and cancer: Late and/or delayed DNA replication timing is associated with increased genomic instability. *Semin. Cancer Biol.*: 1–10
- Donley N & Thayer MJ (2013b) DNA replication timing, genome stability and cancer: late and/or delayed DNA replication timing is associated with increased genomic instability. *Semin. Cancer Biol.* **23**: 80–9
- ENCODE Project Consortium and others (2011) A user's guide to the encyclopedia of DNA elements (ENCODE). *PLoS Biol.* **9**: e1001046
- Felsenfeld G, Boyes J, Chung JAY, Clark D & Studitsky V (1996) Chromatin structure and gene expression. *Proc. Natl. Acad. Sci.* **93**: 9384–9388
- Fritz AJ, Sinha S, Marella N V & Berezney R (2012) Alterations in replication timing of cancer related genes in malignant human breast cancer cells. *J. Cell. Biochem.*: 1–30
- Gauthier M & Bechhoefer J (2009) Control of DNA Replication by Anomalous Reaction-Diffusion

Kinetics. *Phys. Rev. Lett.* **102**: 158104

- Goldar A, Marsolier-Kergoat M-C & Hyrien O (2009) Universal temporal profile of replication origin activation in eukaryotes. *PLoS One* **4**: e5899
- Greenbaum J a, Pang B & Tullius TD (2007) Construction of a genome-scale structural map at single-nucleotide resolution. *Genome Res.* **17**: 947–53
- Hansen RS, Thomas S, Sandstrom R, Canfield TK, Thurman RE, Weaver M, Dorschner MO, Gartler SM & Stamatoyannopoulos JA (2010) Sequencing newly replicated DNA reveals widespread plasticity in human replication timing. *Proc. Natl. Acad. Sci.* **107**: 139–144
- Herrick J, Jun S, Bechhoefer J & Bensimon A (2002) Kinetic model of DNA replication in eukaryotic organisms. *J. Mol. Biol.* **320**: 741–750
- Hiratani I, Leskovar A & Gilbert DM (2004) Differentiation-induced replication-timing changes are restricted to AT-rich/long interspersed nuclear element (LINE)-rich isochores. *Proc. Natl. Acad. Sci. U. S. A.* **101**: 16861–6
- Hiratani I, Ryba T, Itoh M, Rathjen J, Kulik M, Papp B, Fussner E, Bazett-Jones DP, Plath K, Dalton S, Rathjen PD & Gilbert DM (2010) Genome-wide dynamics of replication timing revealed by in vitro models of mouse embryogenesis. *Genome Res.* **20**: 155–69
- Huang DW, Sherman BT & Lempicki RA (2009) Systematic and integrative analysis of large gene lists using DAVID bioinformatics resources. *Nat. Protoc.* **4**: 44–57
- Hyrien O & Goldar A (2010) Mathematical modelling of eukaryotic DNA replication. *Chromosome Res.* **18**: 147–61
- Jun S, Zhang H & Bechhoefer J (2005) Nucleation and growth in one dimension. I. The generalized Kolmogorov-Johnson-Mehl-Avrami model. *Phys. Rev. E* **71**: 011908
- Kolmogorov AN (1937) On the statistical theory of crystallization in metals. *Bull. Acad. Sci. USSR Phys. Ser.:* 355–359
- Lygeros J, Koutroumpas K, Dimopoulos S, Legouras I, Kouretas P, Heichinger C, Nurse P & Lygerou Z (2008) Stochastic hybrid modeling of DNA replication across a complete genome. *Proc. Natl. Acad. Sci. U. S. A.* **105**: 12295–300
- Machida YJ, Hamlin JL & Dutta A (2005) Right place, right time, and only once: replication initiation in metazoans. *Cell* **123**: 13–24
- Martin MM, Ryan M, Kim R, Zakas AL, Fu H, Lin CM, Reinhold WC, Davis SR, Bilke S, Liu H, Doroshov JH, Reimers M a, Valenzuela MS, Pommier Y, Meltzer PS & Aladjem MI (2011) Genome-wide depletion of replication initiation events in highly transcribed regions. *Genome Res.* **21**: 1822–32
- Masai H, Matsumoto S, You Z, Yoshizawa-Sugata N & Oda M (2010) Eukaryotic chromosome DNA replication: where, when, and how? *Annu. Rev. Biochem.* **79**: 89–130
- Meyer LR, Zweig AS, Hinrichs AS, Karolchik D, Kuhn RM, Wong M, Sloan CA, Rosenbloom KR, Roe G, Rhead B, Raney BJ, Pohl A, Malladi VS, Li CH, Lee BT, Learned K, Kirkup V, Hsu F, Heitner S, Harte RA, *et al* (2013) The UCSC Genome Browser database: extensions and updates 2013. *Nucleic Acids Res.* **41**: D64–9
- Moindrot B, Audit B, Klous P, Baker A, Thermes C, de Laat W, Bouvet P, Mongelard F & Arneodo A (2012) 3D chromatin conformation correlates with replication timing and is conserved in resting

cells. *Nucleic Acids Res.* **40**: 9470–81

- De Moura APS, Retkute R, Hawkins M & Nieduszynski C a (2010) Mathematical modelling of whole chromosome replication. *Nucleic Acids Res.* **38**: 5623–33
- Pope BD, Aparicio OM & Gilbert DM (2013) SnapShot: Replication Timing. *Cell* **152**: 1390–1390.e1
- Pruitt KD, Tatusova T & Maglott DR (2005) NCBI Reference Sequence (RefSeq): a curated non-redundant sequence database of genomes, transcripts and proteins. *Nucleic Acids Res.* **33**: D501–4
- Rosenbloom KR, Sloan CA, Malladi VS, Dreszer TR, Learned K, Kirkup VM, Wong MC, Maddren M, Fang R, Heitner SG, Lee BT, Barber GP, Harte RA, Diekhans M, Long JC, Wilder SP, Zweig AS, Karolchik D, Kuhn RM, Haussler D, *et al* (2013) ENCODE data in the UCSC Genome Browser: year 5 update. *Nucleic Acids Res.* **41**: D56–63
- Rowley J (1973) A new consistent chromosomal abnormality in chronic myelogenous leukaemia identified by quinacrine fluorescence and Giemsa staining. *Nature* **243**: 290–3
- Ryba T, Battaglia D, Chang BH, Shirley JW, Buckley Q, Pope BD, Devidas M, Druker BJ & Gilbert DM (2012) Abnormal developmental control of replication-timing domains in pediatric acute lymphoblastic leukemia. *Genome Res.* **22**: 1833–44
- Ryba T, Battaglia D, Pope BD, Hiratani I & Gilbert DM (2011) Genome-scale analysis of replication timing: from bench to bioinformatics. *Nat. Protoc.* **6**: 870–95
- Ryba T, Hiratani I, Lu J, Itoh M, Kulik M, Zhang J, Schulz TC, Robins AJ, Dalton S & Gilbert DM (2010) Evolutionarily conserved replication timing profiles predict long-range chromatin interactions and distinguish closely related cell types. *Genome Res.* **20**: 761–70
- Taylor JH (1960) Asynchronous duplication of chromosomes in cultured cells of Chinese hamster. *J. Biophys. Biochem. Cytol.* **7**: 455–64
- Thurman RE, Rynes E, Humbert R, Vierstra J, Maurano MT, Haugen E, Sheffield NC, Stergachis AB, Wang H, Vernet B, Garg K, John S, Sandstrom R, Bates D, Boatman L, Canfield TK, Diegel M, Dunn D, Ebersol AK, Frum T, *et al* (2012) The accessible chromatin landscape of the human genome. *Nature* **489**: 75–82
- Todd AK, Johnston M & Neidle S (2005) Highly prevalent putative quadruplex sequence motifs in human DNA. *Nucleic Acids Res.* **33**: 2901–7
- Tomlins S a, Rhodes DR, Perner S, Dhanasekaran SM, Mehra R, Sun X-W, Varambally S, Cao X, Tchinda J, Kuefer R, Lee C, Montie JE, Shah RB, Pienta KJ, Rubin M a & Chinnaiyan AM (2005) Recurrent fusion of TMPRSS2 and ETS transcription factor genes in prostate cancer. *Science* **310**: 644–8
- Valenzuela MS, Chen Y, Davis S, Yang F, Walker RL, Bilke S, Lueders J, Martin MM, Aladjem MI, Massion PP & Meltzer PS (2011) Preferential localization of human origins of DNA replication at the 5'-ends of expressed genes and at evolutionarily conserved DNA sequences. *PLoS One* **6**: e17308
- Wiemels JL, Alexander FE, Cazzaniga G, Biondi A, Mayer SP & Greaves M (2000) Microclustering of TEL-AML1 translocation breakpoints in childhood acute lymphoblastic leukemia. *Genes. Chromosomes Cancer* **29**: 219–28
- Yang SC-H & Bechhoefer J (2008) How *Xenopus laevis* embryos replicate reliably: investigating the random-completion problem. *Phys. Rev. E. Stat. Nonlin. Soft Matter Phys.* **78**: 041917

Yang SC-H, Rhind N & Bechhoefer J (2010) Modeling genome-wide replication kinetics reveals a mechanism for regulation of replication timing. *Mol. Syst. Biol.* **6**: 404

Figure Legends

Figure 1

Mechanistic model overview and simulation results. (A) Mechanistic model inputs are Initiation Probability Landscape (IPLS) and the number N of replication forks. The DNA replication program is executed on a simulated cell population (a single cell is depicted). Simulated cells can be either in a non-replicating state (denoted as "G") or a replicating state ("S"). At the start of the simulation all cells are in the G state. Transition from G to S occurs randomly. When in the S state, free (red) rate limiting forks select a random location and bind with a probability set by the IPLS or remain unengaged otherwise. Once engaged (green), replication occurs bi-directionally until forks collide returning to their unengaged state, restarting the process until the genome is replicated. The model periodically queries each cell's replication progress. Once the genome is replicated, the cell enters G state, repeating the process until simulation is terminated. **(B)** Simulated and empirical DNA replication timing are highly correlated. Each point in the contour plot represents a replication time assignment for a 500nt bin on chromosome 12 of GM06990 cells. Simulated replication timing assignment is given on the y-axis and the experimentally derived assignment is given on the x-axis. Contour lines are meant to aid in interpretation. R value represents Pearson's correlation between simulated and empirical data. **(C)** Simulation based on DNase HS sites produces high-fidelity replication timing predictions. The simulated timing program (red) generally lies on or between two experimental datasets plotted on the same axes, the Hansen (Han) dataset (red) and the Ryba (Ryb) dataset (blue). The density of DNase HS sites (DNase I) is plotted with higher density regions colored darker. The stated correlation R values and all the data that are shown is specific to chromosome 14.

Figure 2

DNase HS sites are main independent determinants of DNA replication timing. (A) Simulations based on genome sequence features (GC content, CpG islands), or local genome conformation (ORChID, G-quadruplex), RefSeq annotated transcription start sites (TSS) and gene expression levels (where available) in five cell lines. Shown is the correlation with the Hansen (Han) dataset averaged over 22 autosomal chromosomes, error bars represent the standard error of the mean. **(B)** Mutual independence of representative top-ranking ENCODE marks (DNase, JunD, H3K4me2, H3K9ac) is probed by eliminating co-localized genomic marks in pairwise comparisons. The results of these 4 (datasets) * 3 (overlaps) = 12 sets of simulations are presented in a 4x4 matrix format: rows indicate

the dataset that was used to generate the IPLS, columns indicate the subtracted dataset. Each panel plots the correlation to the experimental timing data in K562 cells (the only set for which all annotations were available) for the full dataset (red), the non-co-localized marks (green) and a “random” dataset (blue) from which the same number of (not necessarily overlapping) marks was removed. Error bars represent standard error of the mean. **(C)** The number of initiation sites had been shown earlier to be non-trivially distributed across chromosomes (Besnard *et al*, 2012). Comparison of the number of DNase HS sites in IMR90 and HELA with the number of initiation sites on each chromosome reveals a tight correlation between the two. Each data-point in the plot represents the fraction (sum = 1) of initiation and DNase HS sites, respectively, on a autosomal chromosome (see also **Fig. S6**).

Figure 3

Mechanistic model is highly reflective of the underlying DNA replication timing biology. (A)

Hierarchical clustering and correlations heatmap of simulated and empirical data. Individual correlations (Pearson's) are noted in the matrix for every dataset pair. Simulations are consistently placed closest to the associated experimental data. The stated correlations are based on simulations which were not optimized for flow-sorter settings. **(B)** Analysis of timing plasticity between simulated GM06990 and K562 cells identified, among other regions, differential timing in the β -globin locus (indicated by dashed lines, genes marked in blue). Hansen dataset (Han) is shown for reference. **(C)** A translocation event simulated *in silico* in GM06990 cells qualitatively reproduces the timing discontinuity observed (Wiemels *et al*, 2000) at a *TEL-AML1* translocation in ALL. Replication profile of translocated (blue line) and normal (red line) are shown on the same genomic axis, the dashed line signifies the translocation coordinate. **(D)** DNA replication timing profiles were simulated using IPLSs derived from GM06990 DNase HS data, noting the number of replication factors that produced highest correlation for each chromosome. Solid line represents a linear fit (shading area denotes the 95% confidence interval). The linear regression curve estimates that the number of forks per megabase is given by $N = 10.24 + 7.9E-7 * x$, where x is chromosome length. The Pearson correlation between the optimal number of replication forks and chromosome length is 0.92. **(E)** Histogram illustrating the distribution of the lengths of the S-phase in a simulated asynchronous cycling population of GM06990 cells.

Table 1: Top DNA Replication Timing Predicting IPLS Sources

IPLS Source	Average Correlation
DnaseDgf	0.865
CCNT2	0.855
JunD	0.855
FaireSeq	0.854
ZNF384	0.849
COREST	0.849
CEBPB	0.847
MAZ	0.842
TBLR1	0.839
eGFP-JunD	0.835
ZNF-MIZD-CP1	0.834
H3K9acB	0.829
H3K4me2	0.829
HCFC1	0.828
UBTF	0.828
HMG3	0.828
BHLHE40	0.827
TBP	0.827
DnaseSeq	0.825
H3K4me1	0.824

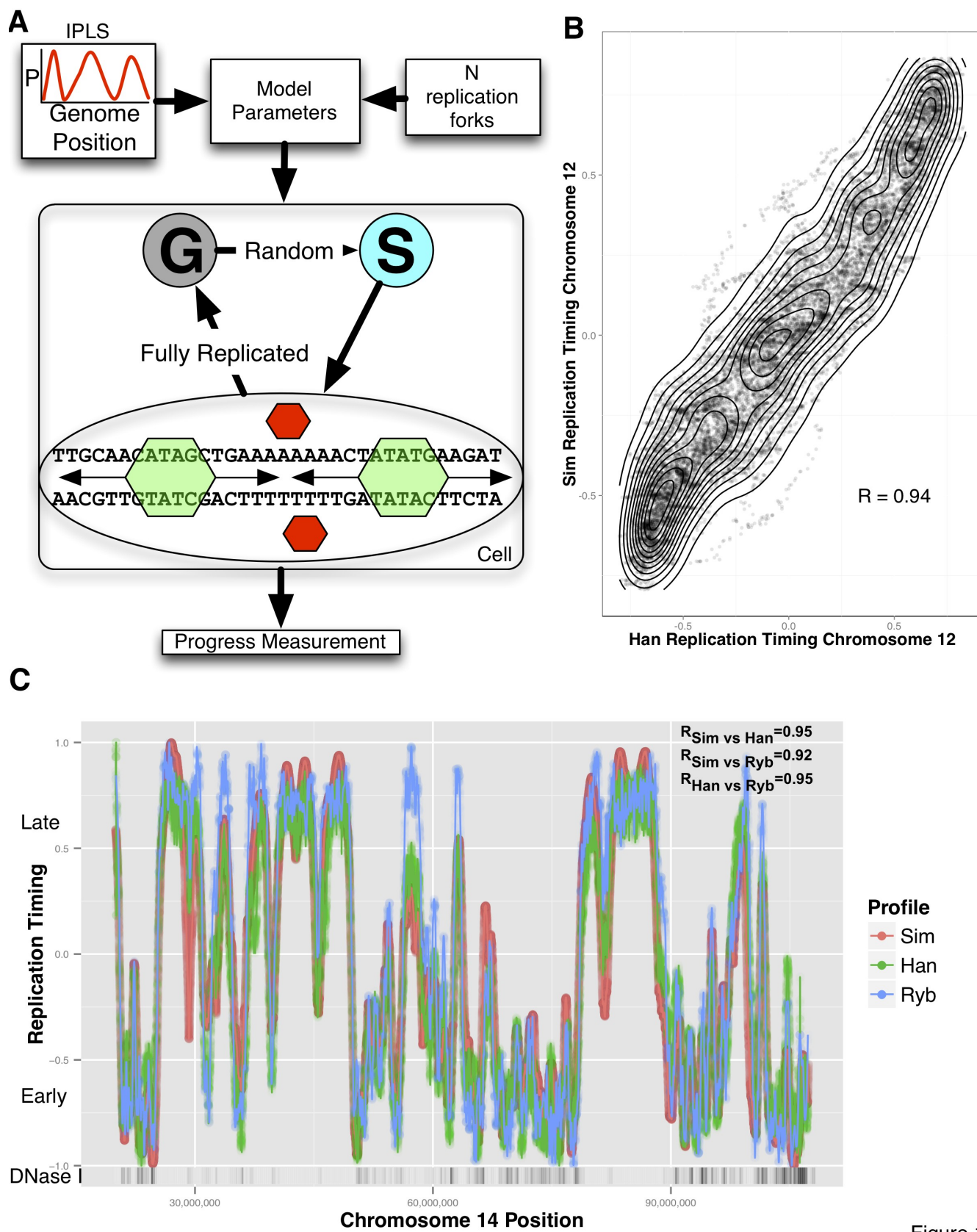


Figure 1

Fig 1.

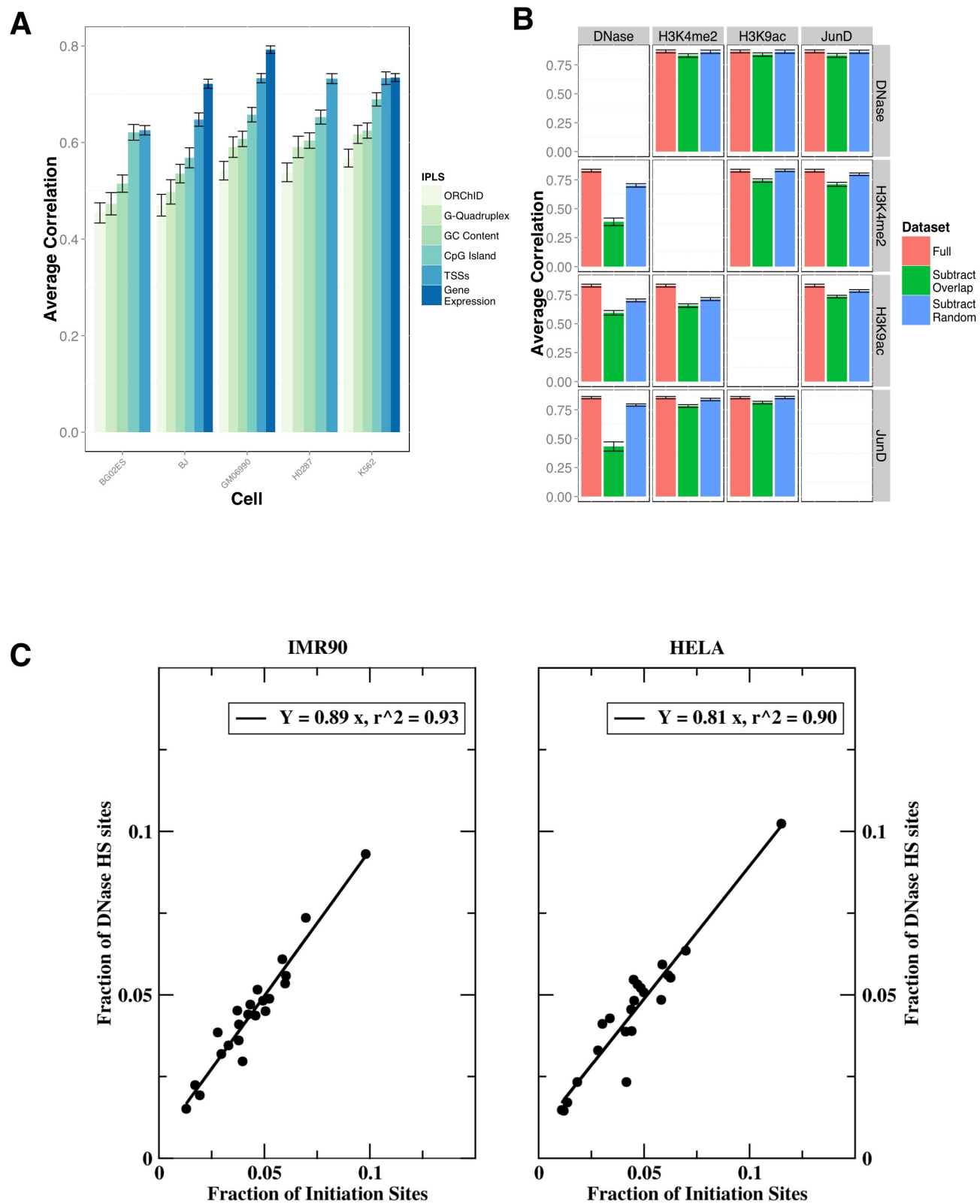


Figure 2

Fig 2.

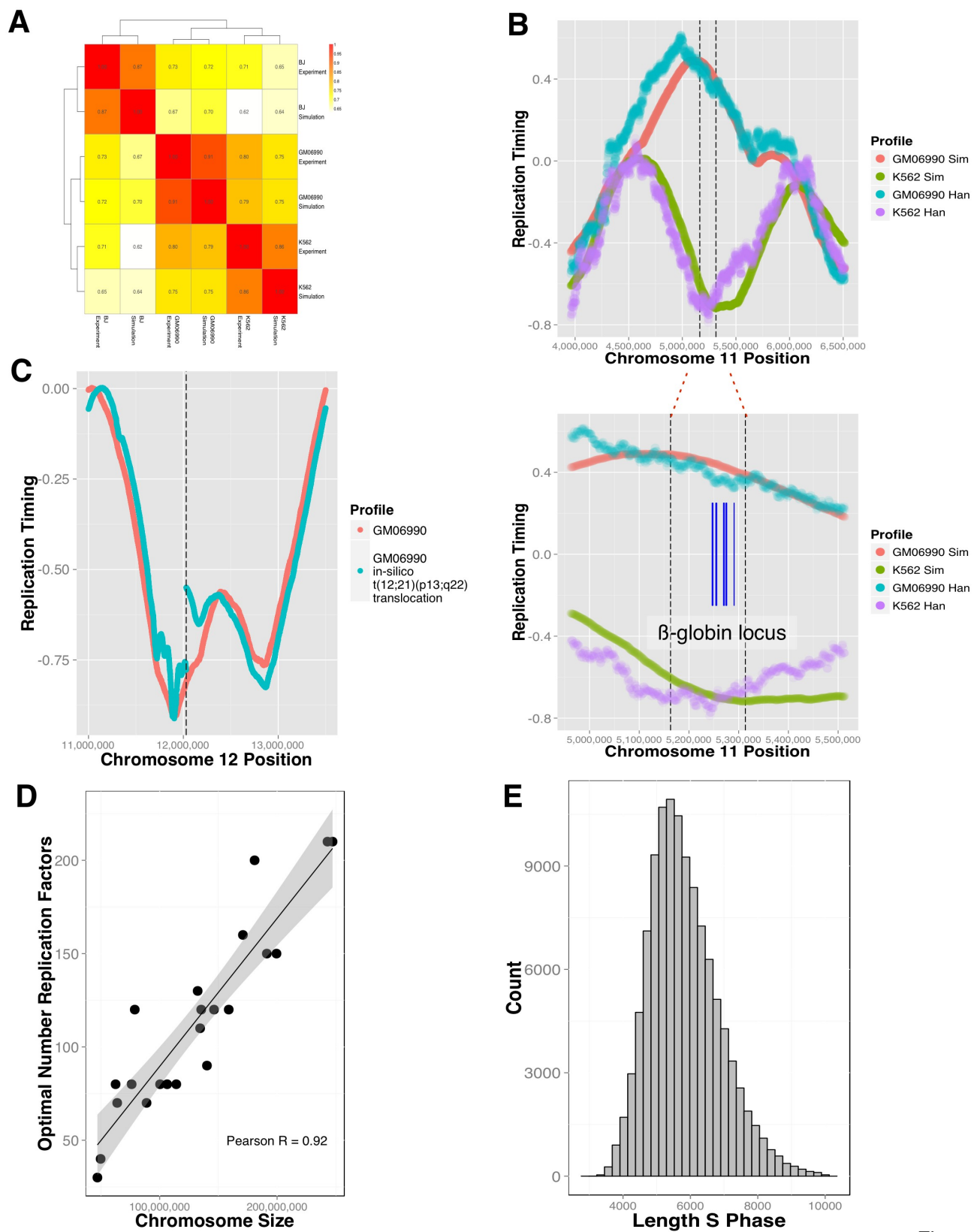


Figure 3

Fig 3.